IOP Publishing Journal of Physics D: Applied Physics
J. Phys. D: Appl. Phys. **49** (2016) 245305 (8pp) doi:10.1088/0022-3727/49/24/245305

The structural evolution of hydrogenated silicon carbide nanocrystals: an approach from bond energy model, Wang–Landau method and first-principles studies

Ya-Ting Wang[1], Yu-Jun Zhao[1,2] and Xiao-Bao Yang[1,2]

[1] Department of Physics, South China University of Technology, Guangzhou 510640, People's Republic of China
[2] Key Laboratory of Advanced Energy Storage Materials of Guangdong Province, South China University of Technology, Guangzhou 510640, People's Republic of China

E-mail: scxbyang@scut.edu.cn

Received 20 December 2015, revised 12 April 2016
Accepted for publication 26 April 2016
Published 18 May 2016

Abstract

The novel properties of nanomaterials are attributed to their variety of structures, while it is a central task to determine the stable configurations under different environment conditions. Exemplified with the hydrogenated cubic silicon carbide nanocrystals (H-SiCNCs), we propose an efficient approach to determine the stable H-SiCNCs by the convex analysis with the possible candidates pre-screened by the Wang–Landau method and a bond energy model, followed by the property analysis from first-principles. We find that the configurations of H-SiCNCs are dominated by the hydrogen and carbon chemical potentials according to the phase diagram, and there are structural transitions with the increasing size from tetrahedron, hexahedron, to octahedron. The energy gaps of tetrahedral H-SiCNCs are larger than that of octahedral ones at similar sizes, and in hexagonal ones there is a charge separation for the highest occupied molecular orbitals and lowest unoccupied molecular orbitals.

Keywords: Wang–Landau method, convex analysis, phase diagram, first-principles calculations

(Some figures may appear in colour only in the online journal)

1. Introduction

Due to potential applications in novel nano-devices, low-dimensional semiconductor nanostructures have been greatly attractive and intensively investigated [1]. Various hydrogenated group-IV nanocrystals (NCs) with sp^3 hybridizations, such as diamond-NCs [2] and silicon-NCs [3], have been considered as the ideal model to demonstrate the quantum-confinement effect [4–6], verified by experimental observations on the electronic properties [7]. Recent studies showed that silicon carbide nanocrystals (SiCNCs) have bright photoluminescence with a high quantum yield of 17% [8, 9], indicating potential applications *in vivo* imaging in biomedicine [10] and fluorescent biological labels [9] due to good biocompatibility [11, 12]. Hydrogenated SiCNCs (H-SiCNCs) with the size from 1 to 6 nm would emit UV-blue light [5], while the glycerol-bonded ones with similar sizes would exhibit broad and stable violet to blue–green emission [13].

Generally, the properties of nanostructures are dominated by the details of structure, such as the sizes, shapes and surface states [14–16]. According to the Wulff construction, the equilibrium crystal shape is determined by surface energies which can be predicted by the first-principles method, depending on the chemical potential [17]. Theoretical calculations [18] showed that the C-terminated SiC-NCs have larger gaps, while the gap of SiCNCs systematically decrease when the surfaces terminated by Si under the H-poor condition. In addition, the gaps of SiC-NCs would decrease as the size increases due to

the quantum confine effect [19]. However, it is still a challenge to determine the stable nanostructures of SiCNCs from numerous possible candidates. Note that there are over 200 crystalline structures for SiC with varying stacking sequences, in which the most important ones are 3C (pure cubic stacking) and 6H, 4H structures which exhibit a hexagonal symmetry with ABCB and ABCAB stack sequences respectively (we herein focus on H-SiCNCs with 3C stacking). On the other hand, the calculation of total energy is essential for the stability valuation and most time-consuming. To reduce the time cost, recent studies calculated the energies using classical potential in Hansel–Vogel (HV) formalism and searched the magic structures of group-IV nanostructures using genetic algorithms [20, 21].

In our previous studies [22, 23], we have demonstrated an effective model for the group-IV nanostructures and confirmed the magic diamond nanocrystals experimentally observed ($C_{10}H_{16}$, $C_{14}H_{20}$, $C_{18}H_{24}$, and $C_{22}H_{28}$) [24]. Searching the ground states of diamond-NCs and silicon-NCs can be achieved by the conventional stochastic algorithm, since the free energies are dominated by the number of H atoms and the stable nanostructures are determined as a function of H chemical potential for given carbon/silicon atoms [22, 23]. However, the model analysis of H-SiCNCs' free energies is expected to be much more complicated, since the chemical potential of carbon and silicon atoms should also modulate the structural stabilities of H-SiCNCs. The parameters' scanning for the phase diagram would induce expensive cost of computation, although the most stable H-SiCNCs could be found by simulated annealing with the traditional Monte-Carlo method for given chemical potentials in principle.

In this paper, we have adopted the Wang–Landau method [25, 26] to screen possible candidates of H-SiCNCs by the bond energy model and determined the stable H-SiCNCs with the convex analysis. The ground states of H-SiCNCs are dominated by the hydrogen and carbon chemical potentials, and the phase diagram indicates the dramatic shape evolution from octahedron to tetrahedron as the size increases. Both gap variations and charge distributions could be tuned by the shapes and sizes of H-SiCNCs.

2. Computational methods

In general, the stable structures of H-SiCNCs could be determined by the analysis of phase diagram as a function of hydrogen/carbon chemical potential (μ_H/μ_C), according to the total energies from the first-principles calculations. However, the proper descriptor of configuration's stabilities should be critical to enhance the screening efficiency of possible candidates, which is an important complement to the first-principles calculations for stability determination. In our previous studies, the cohesive energy of hydrogenated group-IV nanocrystals X_mH_n ($X = C, Si$) can be calculated [22, 23] as $E_{coh} = (2m - 0.5n)E_{X\text{–}X} + nE_{X\text{–}H}$, where $E_{X\text{–}X}(E_{X\text{–}H})$ is the bond energy of X–X (X–H) pair, respectively. The number of H atoms n can be used to distinguish the unequivalent candidates with the same number of X atoms, since the cohesive energies are determined by n. Similarly, the cohesive energy of H-SiCNCs ($Si_{N-m}C_mH_n$) can be expressed as $E_{coh} = n_{Si\text{–}C}E_{Si\text{–}C} + n_{Si\text{–}H}E_{Si\text{–}H} + n_{C\text{–}H}E_{C\text{–}H}$, where N is the total number of carbon and silicon atoms, $E_{Si\text{–}C}/E_{Si\text{–}H}/E_{C\text{–}H}$ are the bond energies of Si–C/Si–H/C–H, and $n_{Si\text{–}C}/n_{Si\text{–}H}/n_{C\text{–}H}$ are the number of Si–C/Si–H/C–H bonds, respectively. Considering that there are four nearest neighbors for C and Si atoms, we have $n_{Si\text{–}H} = 4(N - m) - n_{Si\text{–}C}$ and $n_{C\text{–}H} = 4m - n_{Si\text{–}C}$.

Given N for the total number of C and Si atoms, the most stable structures could be found by simulated annealing with the traditional Monte-Carlo method for each given chemical potential of C/H atoms. However, the parameters' scanning for the phase diagram would induce expensive cost of computation. On the other hand, the cohesive energy of $Si_{N-m}C_mH_n$ are determined by the number of Si–C bonds ($n_{Si\text{–}C}$) and C atoms (m). Thus, the unequivalent candidates are distinguished by the order pair of ($n_{Si\text{–}C}$, m), which would greatly enhance the efficiency if these unequivalent candidates can be symmetrically pre-screened. In the Wang–Landau method, the accepted probability of the transmission among different structures are reciprocal to the degenerate degree of system (while degenerate degree can be persistently modified in the process of searching and convergence finally), allowing most of the unequivalent structures to be visited at the same probability. Without the parameters' scanning, we can determine the stable structures from the whole unequivalent candidates according to the phase diagram of chemical potential, by either the bond energy model or first-principles calculations.

We performed the calculation of total energies for various H-SiCNCs by the density-functional theory (DFT) method implemented in the Vienna *ab initio* simulation package [27–30] (VASP). The projector augmented wave (PAW) method was adopted and the exchange-correlation functional was in the form of Perdew–Burke–Ernzerhof (PBE) within the generalized gradient approximation (GGA). The energy cutoff was set to be 450 eV with a k-point mesh of $1 \times 1 \times 1$ and the vacuum distance was 10 Å, ensuring the convergence of the forces on each atom was less than 0.01 eV Å^{-1}. For electronic properties, we focused on the energy gaps between the highest occupied molecular orbitals (HOMOs) and the lowest unoccupied molecular orbitals (LUMOs). Since the GGA calculation underestimates the band gaps of semiconductors compared to the experimental results, we also performed the calculations with the function of Heyed–Scuseria–Ernzerhof (HSE06) [31–34]. The HSE06 calculated band gap for bulk 3C-SiC was 2.24 eV which is in good agreement with the experiment results [35]. Due to the expensive computational cost, we only employed the function of HSE06 for the HOMO-LUMO gap calculation of small H-SiCNCs.

3. Results and discussions

We have screened the possible candidates of small H-SiCNCs with the Wang–Landau method and determined the ground states by the phase diagram from first-principles calculations, as shown in section 3.1. In section 3.2, we considered the structural evolution of large H-SiCNCs with typical shapes,

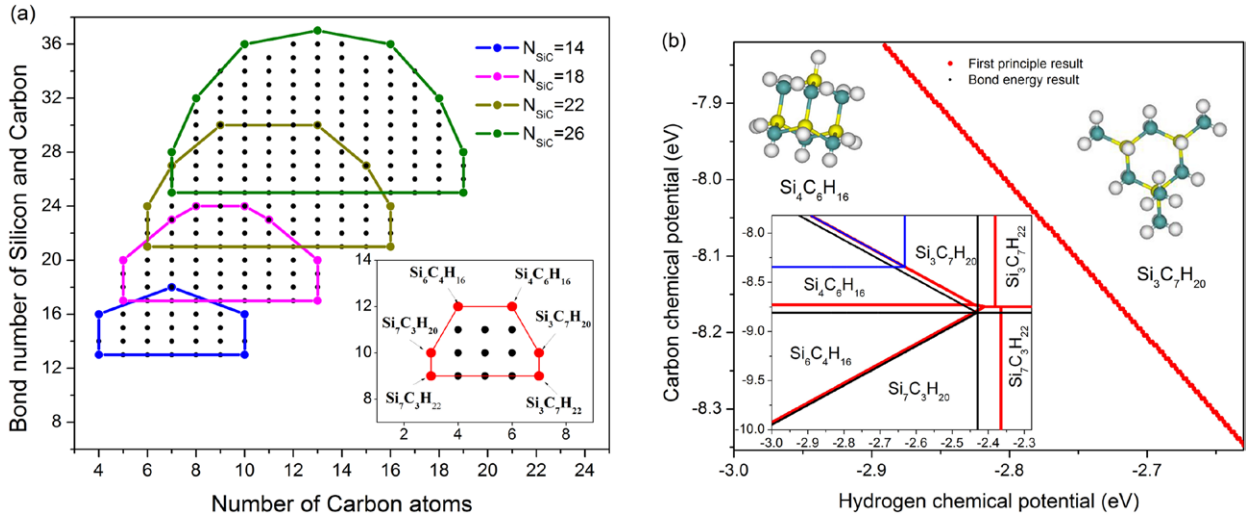

Figure 1. Convex analysis and phase diagram for H-SiCNCs with various sizes. (a) Possible ($n_{\mathrm{Si-C}}$, m) for $Si_{N-m}C_mH_n$, $N = 14$, 18, 22, 26 and the inset shows the case of $N = 10$; (b) phase diagram for $Si_{10-m}C_mH_n$ as a function of carbon and hydrogen chemical potential. Yellow, cyan and white balls represent Si, C and H respectively.

with respect to the variations of the hydrogen/carbon chemical potentials. The electronic properties of the H-SiCNCs, including the gaps and the charge distributions of near-gap levels, are discussed in section 3.3.

3.1. Screening candidates with Wang–Landau method

As shown in figure 1(a), we obtained the unequivalent candidates of $Si_{N-m}C_mH_n$ (for $N = 10$, 14, 18, 22, and 26), with various number of $n_{\mathrm{Si-C}}$ and m. Taking $N = 10$ for an example, there are 15 unequivalent candidates with six convexes, as shown in the inset of figure 1(a). The formation energy of $Si_{N-m}C_mH_n$ can be calculated as $E_f = (-E_{coh} - (N-m)\mu_{Si} - m\mu_C - n\mu_H)/N$, where μ_H, μ_C and μ_{Si} are chemical potentials of H, C and Si atoms. As shown in the inset of figure 1(b), there are six stable structures according to the phase diagram with $\mu_H \in [-3.0, -2.3]$ eV and $\mu_C \in [-10, -7.8]$ eV, where the results from the bond energy model and first-principles calculations are shown in black and red respectively. Although there are some deviations in the boundaries of the phase diagram, six ground states correspond to the convexes of $Si_6C_4H_{16}$, $Si_4C_6H_{16}$, $Si_7C_3H_{20}$, $Si_3C_7H_{20}$, $Si_7C_3H_{22}$ and $Si_3C_7H_{22}$ (shown in the inset of figure 1(a)). Thus, we can determine the stable structures of H-SiCNCs in a simple and fast way, which are in agreement with the first-principles calculations. Our candidate screening by the Wang–Landau method and the convex analysis is found to be of high efficiency, though the number of candidates would grow fast as the size increases,

There are several constrains for μ_H, μ_C, and μ_{Si}: (i) $\mu_{Si} + \mu_C = \mu_{\mathrm{SiC\text{-}bulk}}$, where $\mu_{\mathrm{SiC\text{-}bulk}}$ is obtained from the chemical potential of bulk SiC; (ii) μ_C and μ_{Si} should be less than the chemical potential of bulk diamond and silicon; (iii) $\mu_H \leqslant (\mu_{CH_4} - \mu_C)/4$, $\mu_H \leqslant (\mu_{SiH_4} - \mu_C)/4$, and $\mu_H \leqslant \mu_{H_2}/2$, where μ_{H_2}, μ_{CH_4} and μ_{SiH_4} are the chemical potential of H_2, CH_4, and SiH_4 at the gas phase. Thus, we have $-8.35\,\mathrm{eV} \leqslant \mu_C \leqslant -7.82\,\mathrm{eV}$ and $\mu_H \leqslant -2.63$ eV. Considering the above constrains, we found two stable structures of $Si_4C_6H_{16}$ and $Si_3C_7H_{20}$ in the phase diagram, which corresponds to the areas marked by blue shown in the inset of figure 1(b). For small H-SiCNCs, the chemical potential of Si and C atoms might not satisfy the equilibrium condition of bulk 3C-SiC. Thus, six stable structures at the convexes in the inset of figure 1(a) might be observed experimentally by the control of chemical potential without constraint. The unique structure of $Si_4C_6H_{16}$ is the same as that of adamantane ($C_{10}H_{16}$) with the symmetry of T_d, corresponding to the one with the least hydrogen atoms for the diamond-NCs containing ten carbon atoms. The maximal H number is $2N + 2$ for $Si_{N-m}C_mH_n$ with $N = 10$, and $Si_3C_7H_{20}$ have a hexagonal ring which reduces the hydrogen number by 2. Both these two stable structures of $Si_4C_6H_{16}$ and $Si_3C_7H_{20}$ contain more C atoms than Si atoms.

Similarly, we have screened the candidates of $Si_{N-m}C_mH_n$ with $N = 14$, 18, 22 and 26, through the Wang–Landau method. Figure 2 shows the stable structures and the phase diagram as a function of the chemical potential of carbon and hydrogen atoms. For $N = 14$, there are five convex and the corresponding structures are $Si_7C_7H_{20}$, $Si_4C_{10}H_{24}$, $Si_{10}C_4H_{24}$, $Si_4C_{10}H_{30}$, and $Si_{10}C_4H_{30}$ (shown in figure 1(a)). According to the phase diagram, the stable structures are $Si_7C_7H_{20}$ and $Si_4C_{10}H_{24}$ (shown in figure 2(a)). The shape of $Si_4C_{10}H_{24}$ is a tetrahedron with the symmetry of T_d, while $Si_7C_7H_{20}$ is a hexahedron with the symmetry of D_{3d} as the diamantane of $C_{14}H_{20}$. Note that both the structures of $Si_4C_{10}H_{24}$ and $Si_7C_7H_{20}$ are unique with no isomer.

As shown in figures 2(b)–(d), the structures of $Si_8C_{10}H_{24}$, $Si_9C_{13}H_{28}$, $Si_{10}C_{16}H_{32}$ and $Si_{13}C_{13}H_{30}$ are unique. The structures of $Si_8C_{10}H_{24}$ and $Si_9C_{13}H_{28}$ are the same as that of triamantane and tetramantane with the symmetry of C_{2v} and C_{3v} respectively, which correspond to the ones with the least hydrogen atoms for the diamond-NCs. As the hydrogen chemical potential increases, the structures with more hydrogen atoms would also be stable. For example, $Si_{13}C_{13}H_{30}$ is a hexahedron with the symmetry of D_{3d}, while the tetrahedral $Si_{10}C_{16}H_{32}$ with the symmetry of T_d would become more stable with the

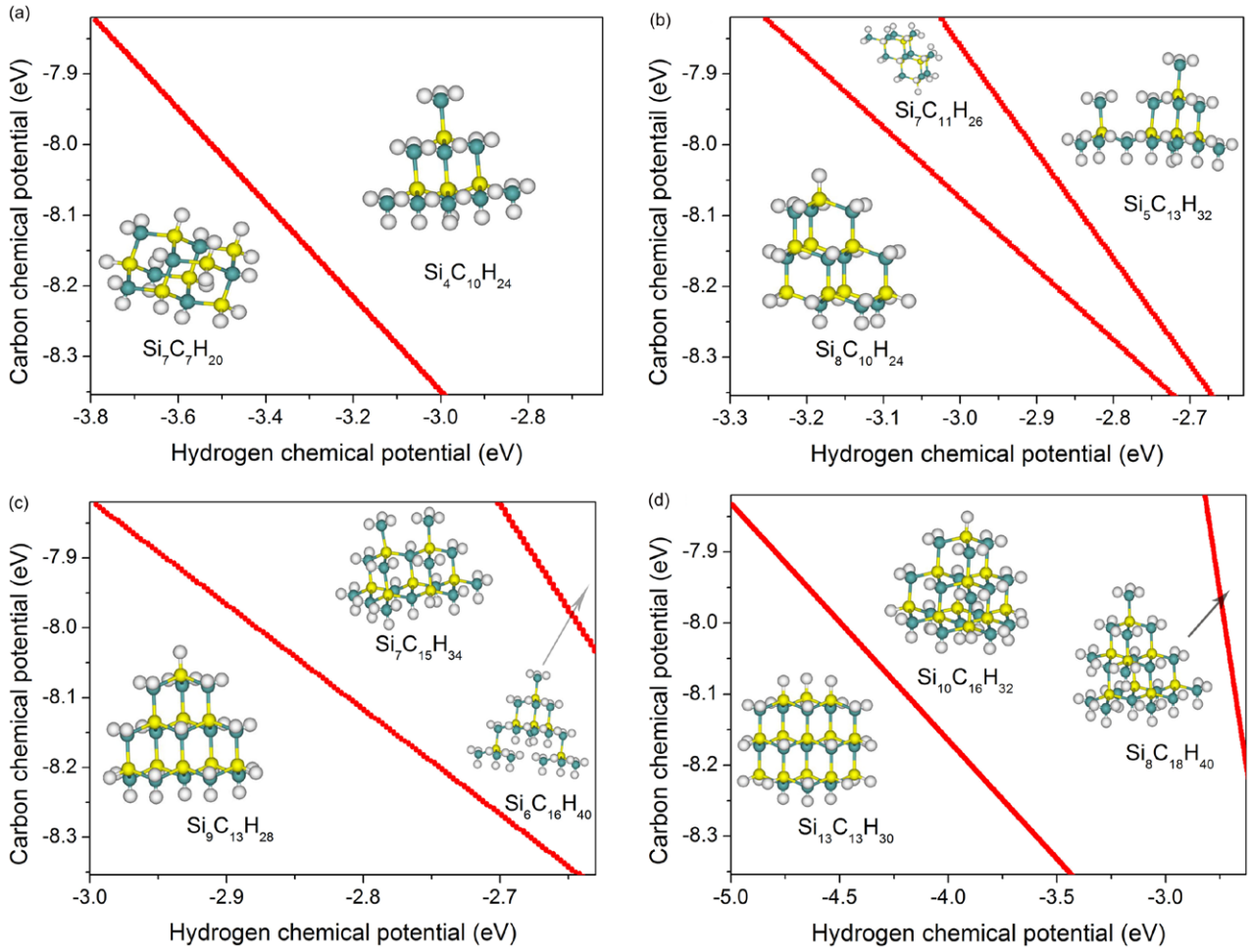

Figure 2. Phase diagrams and stable H-SiCNCs of $Si_{N-m}C_mH_n$, for $N = 14, 18, 22, 26$. The hydrogen chemical potential is less than -2.63 eV and the range of carbon chemical potential is -8.35 eV to -7.82 eV. Yellow, cyan and white balls represent Si, C and H respectively.

increasing of hydrogen and carbon chemical potentials. Note that the number of C atoms is greater than or equal to that of Si atoms in all these stable structures, where the surfaces are mainly occupied by C atoms instead of Si atoms. For small diamond-NCs experimentally found [24], there are no surface reconstructions and thus we focus on the stable H-SiCNCs without surface reconstructions in the following.

3.2. Shape evolution of H-SiCNCs

As shown above, we have determined the ground states of small H-SiCNCs combining the first-principles calculations with the Wang–Landau method, demonstrating the shape evolution with various symmetries of $Si_{N-m}C_mH_n$, such as tetrahedron and hexahedron, whose surfaces are mainly enclosed by the (1 1 1) facets. Thus, we focus on three typical kinds of H-SiCNCs in the shape of tetrahedron, hexahedron and octahedron, where the truncated tetrahedron and octahedron clusters as the spherical structures are also considered for comparison. The formula for the hexahedron H-SiCNCs is $\mathrm{Si:C:H} = n^3 + 3n^2 + 3n : n^3 + 3n^2 + 3n : 6n^2 + 12n + 2$, where the number of Si and C atoms is the same. The formulas are $\mathrm{Si:C:H} = {}^{n^3}\!/_6 + n^2 + {}^{11n}\!/_6 + 1 : {}^{n^3}\!/_6 + {}^{3n^2}\!/_2 + {}^{13n}\!/_3 : 2n^2 + 10n + 4$ and $\mathrm{Si:C:H} = {}^{2n^3}\!/_3 + 4n^2 + {}^{22n}\!/_3 + 4 : {}^{2n^3}\!/_3 + 4n^2 + {}^{25n}\!/_3 + +6 : 4n^2 + 16n + 16$ for the tetrahedron and octahedron respectively, where the number of Si and C atoms can be exchanged to obtain the other kinds of H-SiCNCs with the same shape. Due to the computational expense, we focused on the clusters with the total number of Si/C atoms less than 300, where the number n is in the range of [1, 4] for hexahedron and octahedron, in [1, 7] for tetrahedron.

As shown in figure 3(a), we have demonstrated the shape evolution of SiC-NCs as the size increases, in various carbon chemical potential and hydrogen chemical potential. All the stable H-SiCNCs contain more C atoms than Si atoms, and there are three regions (I, II, III) in the phase diagram, where the interpolation method has been applied to determine the boundary. In region I, the octahedron clusters are more stable compared to the tetrahedron and hexahedron ones, while the tetrahedron clusters are most stable in region III. Under the chemical potential of C and H in these two regions, the shape would be uniform in either octahedron or tetrahedron as the size increases. In region II, there would be concurrence of tetrahedron and octahedron H-SiCNCs, depending on the sizes of clusters. For given chemical potential of C and H, the shape of H-SiCNCs would be changed from tetrahedron to

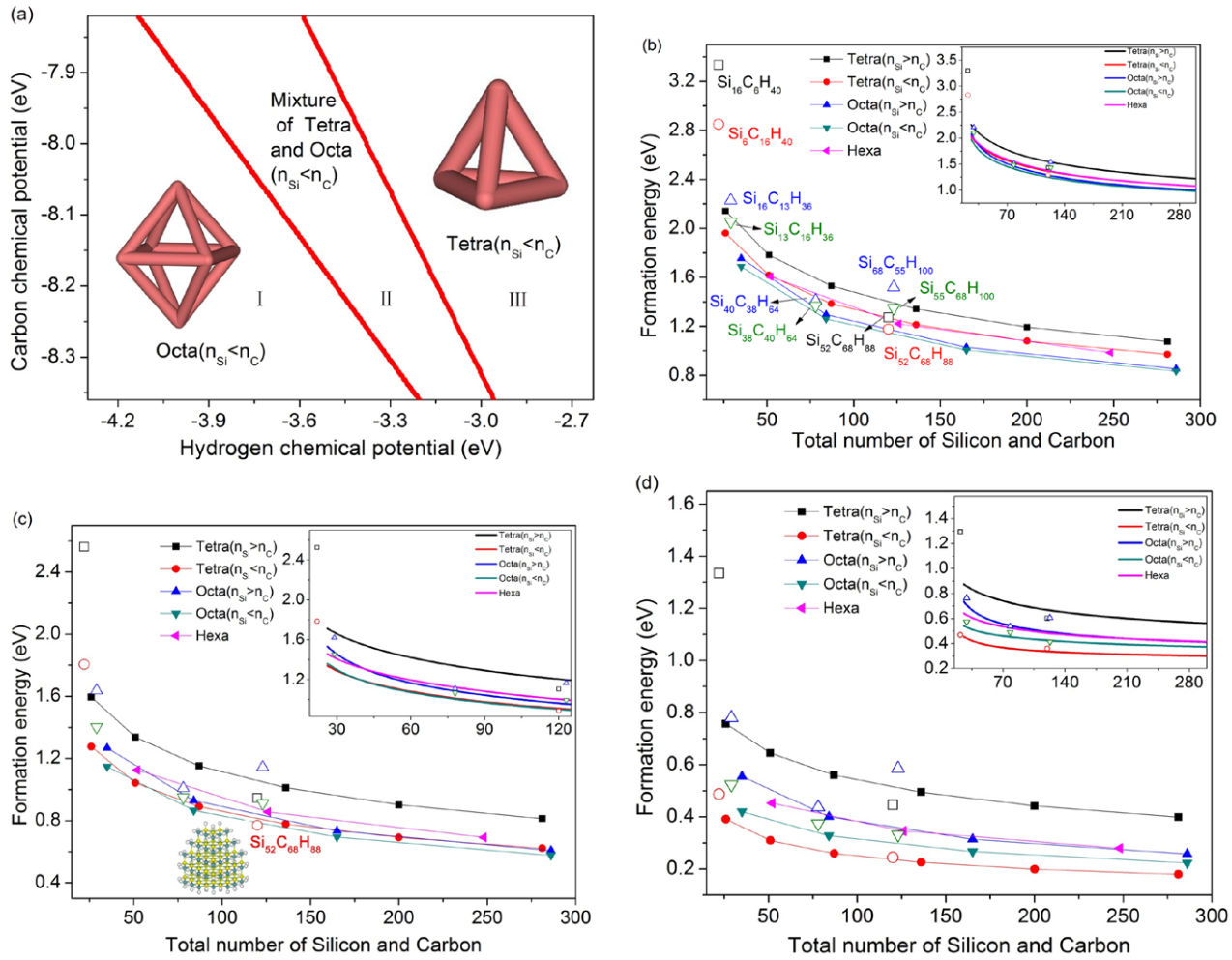

Figure 3. Shape evolution of H-SiCNCs as a function of size and chemical potentials. (a) Phase distributions as a function of carbon and hydrogen chemical potential; (b)–(d) formation energy as a function of the total number of silicon and carbon. The black, red, blue and olive empty shapes are spherical clusters which are derived from truncated tetrahedron ($n_{Si} > n_C$ and $n_{Si} < n_C$) and octahedron ($n_{Si} > n_C$ and $n_{Si} < n_C$). These three grams are obtained by first-principles while the insets are calculated by the bond model. For (b) $\mu_C = -8$ eV, $\mu_H = -4$ eV, for (c) $\mu_C = -8$ eV, $\mu_H = -3.5$ eV, for (d) $\mu_C = -8$ eV, $\mu_H = -2.95$ eV. Yellow, cyan and white balls represent Si, C, and H respectively.

octahedron as the sizes increase. Note that there is no region in which the hexahedron clusters are most stable.

To verify the phase diagram, we showed the variation of formation energies of H-SiCNCs as a function of sizes under certain C and H chemical potentials as shown in figures 3(b)–(d). The total energies of typical H-SiCNCs with various sizes were obtained by the first-principles calculations. Taking $\mu_C = -8$ eV and $\mu_H = -4$ eV in region I of figure 3(a) as an example, the formation energies decrease as the size increases (as shown in figure 3(b)) and the octahedron clusters are almost the most stable structures, in good agreement with the results obtained from the bond energy model shown in the inset of figure 3(b). Although there is a deviation about 0.1 eV in the formation energies compared to the first-principles calculations, the trend predicted by the bond energy model is verified, indicating that the stable structures are the octahedral ones with more C atoms. In region II of figure 3(a) with $\mu_C = -8$ eV and $\mu_H = -3.5$ eV, there is an intersection (around $N = 38$) in the formation energies for octahedron and tetrahedron clusters (shown in the inset of figure 3(c)). According to the results for first-principles calculations, we have found that the tetrahedron H-SiCNCs would become unstable when the total number of C and Si is larger than 38. Note that a spherical cluster ($Si_{52}C_{68}H_{88}$) will be more stable compared to the octahedral and tetrahedral ones. For region III of figure 3(a), the tetrahedral clusters will be the most stable, as confirmed by both the bond energy model and the first-principles calculations (shown in figure 3(d)). Thus, we show the shape evolution of H-SiCNCs as a function of the chemical potentials, where the truncated tetrahedron is found to be a transition structure with a spherical shape between the tetrahedral and octahedral clusters.

3.3. Electronic properties for stable H-SiCNCs

In the following, we would focus on the electronic properties of H-SiCNCs, including the energy gaps and the charge distributions of HOMOs and LUMOs. For small $Si_{N-m}C_mH_n$ with $N < 30$, we have employed the HSE06 method for the calculation of HOMO-LUMO gaps. Figure 4(a) shows

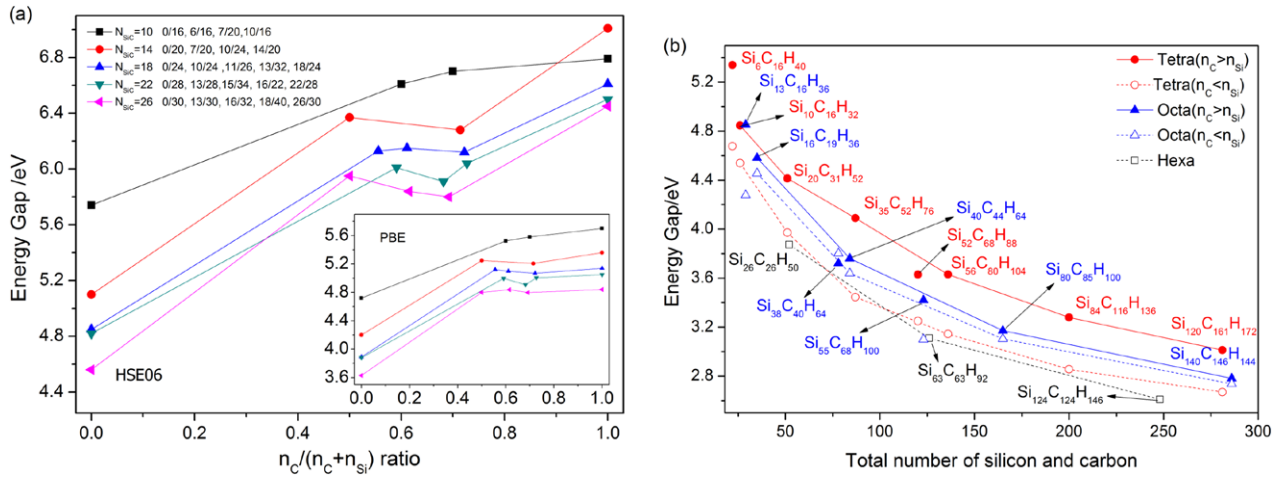

Figure 4. (a) The energy gaps of small H-SiCNCs as a function of $n_C/(n_C + n_{Si})$ ratio calculated with the function of HSE06 and the ones calculated with the function of PBE are shown in the inset. The number of C and H atoms are listed with the increment of C atoms, e.g. 0/16 and 7/20 for $N_{SiC} = 10$ corresponds to $C_0Si_{10}H_{16}$ and $C_7Si_3H_{20}$ respectively. (b) The energy gaps of typical H-SiCNCs as a function of N (total number of silicon and carbon) calculated with the function of PBE. The tetrahedron and octahedron H-SiCNCs with more carbon atoms are presented with full lines, while the other ones are presented with dash lines.

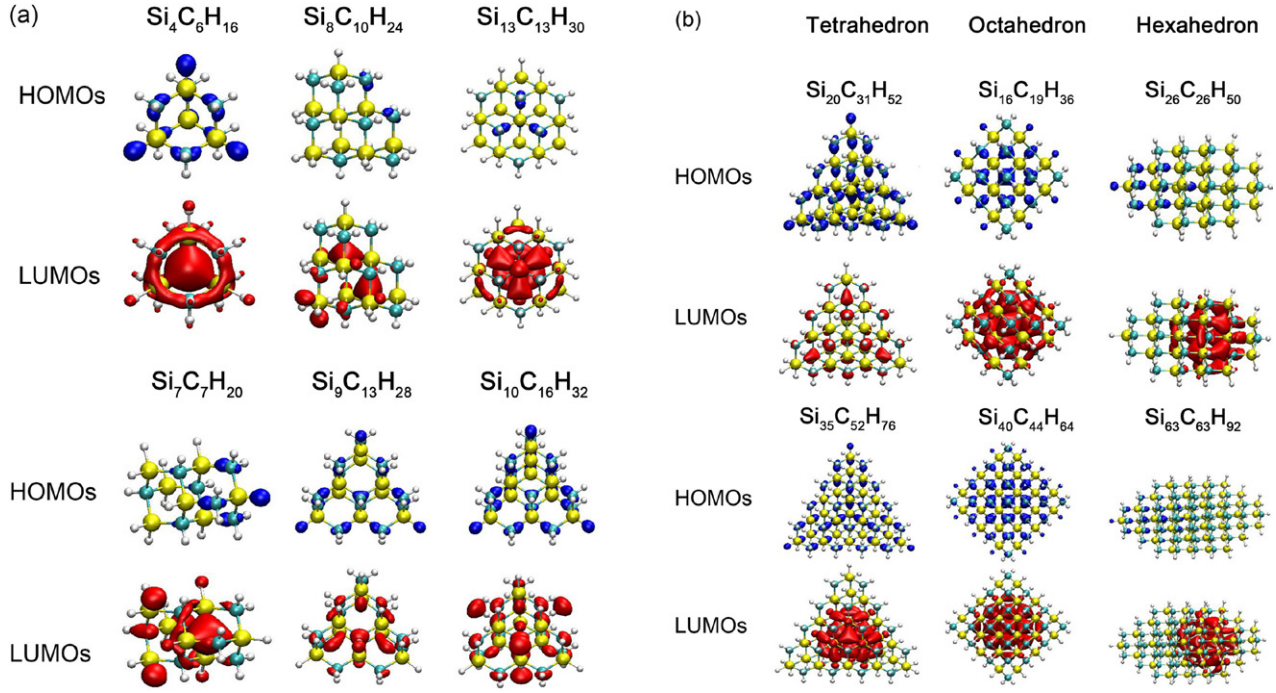

Figure 5. (a) Charge distributions of HOMOs and LUMOs of small H-SiCNCs. The isosurfaces compared to the peak amplitudes are 25%/25%/50%/40%/30% for $Si_4C_6H_{16}$/$Si_7C_7H_{20}$/$Si_9C_{13}H_{28}$/$Si_{13}C_{13}H_{30}$/$Si_{10}C_{16}H_{32}$. (b) Charge distributions of HOMOs and LUMOs of tetrahedral, octahedral and hexahedronal H-SiCNCs. The isosurfaces compared to the peak amplitudes are 30%/35% for tetrahedron (small/large clusters), 40%/30% for octahedron, and 35%/30% for hexahedron. The charge distributions of HOMOs and LUMOs are represented by blue and red respectively. Yellow, cyan and white balls are for Si, C, and H atoms.

the variation of gaps as a function of the ratio of m/N and $m = 0$, N is considered for comparison which corresponds to the diamond and silicon nanocrystals in the same shape respectively. In all cases, the gaps of diamond nanocrystals are largest, while the ones of silicon nanocrystals are smallest. For $N = 10$, the energy gaps increase with the ratio of m/N increases, while the energy gaps have a local maximum at $m/N = 0.5$ for $N = 14$, 26, corresponding to $Si_7C_7H_{20}$ and $Si_{13}C_{13}H_{30}$. For $N = 18$, 22, the local maximum of energy gaps is at around $m/N = 0.6$ and the corresponding structures are $Si_8C_{10}H_{24}$ and $Si_9C_{13}H_{28}$ respectively. The energy gaps from the DFT-GGA/PBE calculations are also shown in the inset of figure 4(a) for comparison, with their values about 1 eV lower than that from the HSE06. Note that both these two methods indicate the similar trend of gaps' variation, though the ones from the HSE06 are more accurate. Due to the expensive cost of computation, we only use DFT-GGA/PBE calculations for larger H-SiCNCs.

Figure 4(b) shows the variation of energy gaps as a function of size for various typical H-SiCNCs including the

spherical structures. The values decrease as the total number of Si and C atoms increase. According to the phase diagram, the tetrahedral and octahedral H-SiCNCs with more C atoms would be more stable under proper hydrogen and carbon chemical potential. We have found that the energy gaps of tetrahedral clusters are larger than that of octahedral and spherical ones, for the clusters with the similar sizes. For comparison, we have also calculated the energy gaps of hexahedral H-SiCNCs, tetrahedral and octahedral ones and their spherical structure with more Si atoms. The gaps of hexahedral ones are smallest for the clusters with the similar sizes. Thus, both the size and shape have an important effect on the energy gaps.

We have also investigated the charge distributions of HOMOs and LUMOs of various H-SiCNCs. For $Si_4C_6H_{16}$, the charge of HOMOs is mainly located around the carbon of Si–C and the hydrogen of Si–H bonds, while the charge of LUMOs is concentrated inside the clusters (shown in figure 5(a)). We have also calculated the charge distributions with the HSE06 method. It is found that no remarkable difference for the LUMOs of $Si_4C_6H_{16}$, though the charge distribution of HOMOs at some H atoms decreases in the HSE06 result (not shown). We did not calculate all the charge distribution of HOMOs and LUMOs with HSE06 due to the expensive computational cost. For $Si_8C_{10}H_{24}$, $Si_9C_{13}H_{28}$ and $Si_{10}C_{16}H_{32}$, the charges of HOMOs are also distributed around the carbon of Si–C and hydrogen of Si–H bonds, while the charges of LUMOs tend to be located around $–SiH_2$/$–CH_2$ besides the inside of clusters. Note that the charge of HOMOs for $Si_{13}C_{13}H_{30}$ is mostly distributed around the C–H bonds, instead of the Si–H bonds.

Similar analysis of HOMOs and LUMOs has been applied to the typical H-SiCNCs. For tetrahedral ones, four surfaces are enclosed by –CH bonds and six edges are by $–CH_2$ bonds with four –SiH at the four vertexes. Taking $Si_{20}C_{31}H_{52}$ and $Si_{35}C_{52}H_{76}$ as examples, the charges of HOMOs are largely around the carbon derived from $–CH_2$ and –CH bonds as shown in figure 5(b). Meanwhile, the charges of LUMOs are mainly distributed inside the clusters and the one for $Si_{35}C_{52}H_{76}$ is more localized compared to $Si_{20}C_{31}H_{52}$. The eight surfaces of octahedral H-SiCNCs are enclosed by both –CH and –SiH bonds. The charges of HOMOs are mainly around the carbon atoms inside and –CH bonds on the edge, while the LUMOs are concentrated inside the clusters, such as $Si_{16}C_{19}H_{36}$ and $Si_{40}C_{44}H_{64}$. Taking $Si_{26}C_{26}H_{50}$ and $Si_{63}C_{63}H_{92}$ as examples for hexahedral H-SiCNCs, the left part is enclosed by –CH bonds and the right one is by –SiH bonds. Interestingly, the charges of HOMOs are mainly distributed on the left and that of LUMOs are concentrated on the right, indicating a charge separation of HOMOs and LUMOs. In general, the spatial charge distributions of HOMOs and LUMOs are crucial in the design of the optical nano-device. It can be achieved by the control of morphology, such as the tapered Si NWs [36, 37]. According to the phase diagram, the hexahedral H-SiCNCs are not ground states compared to the tetrahedral and octahedral ones, which might be obtained by the unequilibrium growth in the experiments.

4. Summary

In summary, we have systematically investigated the structural stabilities of H-SiCNCs through the high efficient approach from first-principles calculations combined with the Wang–Landau method and bond energy model. Without the parameters' scanning, the stable H-SiCNCs for various sizes have been determined with the convex analysis and verified by the first-principles calculations, as the configurations are dominated by the hydrogen and carbon chemical potentials according to the phase diagram. There are three typical regions in the phase diagram indicating the shape evolution from octahedron to tetrahedron for large H-SiCNCs: octahedral and tetrahedral H-SiCNCs are stable in regions I and III respectively, while the shape changes from tetrahedron to octahedron when the total number of C and Si is larger than 38 in region II. The energy gaps of tetrahedral H-SiCNCs are larger than that of octahedral ones at similar sizes, and in hexagonal ones there is a charge separation for HOMOs and LUMOs. Our finding indicates the possibility of designing electronic nanodevices by modulating the configurations with the control of hydrogen and carbon chemical potential. Until now, most SiCNCs observed experimentally are larger than 1 nm in size, which indicates the difficulty of obtaining smaller SiCNCs. However, the novel properties of small SiCNCs might generate experimental interest and efforts to realize such systems, exploring the possible application with the luminescence of small SiCNCs.

Acknowledgments

This work was supported by NSFC (Grant Nos. 11474100 and 11574088) and Guangdong Natural Science Funds for Distinguished Young Scholars (Grant No. 2014A030306024), and the Fundamental Research Funds for the Central Universities (2015PT017, 2015ZP010). The computer times at National Supercomputing Center in Shenzhen (NSCCSZ) and ScGrid of the Super-computing Center, Computer Network Information Center of CAS are gratefully acknowledged.

References

[1] Baletto F and Ferrando R 2005 *Rev. Mod. Phys.* **77** 371–423
[2] Liu S G, Dahl J E and Carlson R M K 2003 *Science* **299** 96–9
[3] Dinh L N, van Buuren T, Chase L L, Siekhaus W J and Terminello L J 1998 *Phys. Rev. Lett.* **80** 3803–60
[4] Öğüt S, Chelikowsky J R and Louie S G 1997 *Phys. Rev. Lett.* **79** 1770–3
[5] Garoufalis C S, Zdetsis A D and Grimme S 2001 *Phys. Rev. Lett.* **87** 276402
[6] Yu T, Pi X, Ni Z, Zhang H and Yang D 2015 *AIP Adv.* **5** 037140
[7] Belomoin G, Therrien J, Smith A, Rao S, Twesten R, Chaieb S, Nayfeh M H, Wagner L and Mitas L 2002 *Appl. Phys. Lett.* **80** 841
[8] Wu X, Fan J, Qiu T, Yang X, Siu G and Chu P 2005 *Phys. Rev. Lett.* **94** 026102
[9] Fan J, Li H, Jiang J, So L K, Lam Y W and Chu P K 2008 *Small* **4** 1058–62
[10] Somogyi B, Zolyomi V and Gali A 2012 *Nanoscale* **4** 7720–6

[11] Fan J and Chu P K 2010 *Small* **6** 2080–98
[12] Serdiuk T, Alekseev S A, Lysenko V, Skryshevsky V A and Geloen A 2012 *Nanotechnology* **23** 315101
[13] Wang J, Xiong S J, Wu X L, Li T H and Chu P K 2010 *Nano Lett.* **10** 1466–71
[14] Delerue C, Allan G and Lannoo M 1993 *Phys. Rev.* B **48** 11024–36
[15] Wang R, Pi X and Yang D 2012 *J. Phys. Chem.* C **116** 19434–43
[16] Ni Z, Pi X, Ali M, Zhou S, Nozaki T and Yang D 2015 *J. Phys. D: Appl. Phys.* **48** 314006
[17] Li H, Geelhaar L, Riechert H and Draxl C 2015 *Phys. Rev. Lett.* **115** 085503
[18] Reboredo F A, Pizzagalli L and Galli G 2004 *Nano Lett.* **4** 801–4
[19] Peng X H, Nayak S K, Alizadeh A, Varanasi K K, Bhate N, Rowland L B and Kumar S K 2007 *J. Appl. Phys.* **102** 024304
[20] Ciobanu C V, Chan T L, Chuang F C, Lu N, Wang C Z and Ho K M 2006 *Nano Lett.* **6** 277–81
[21] Lu N, Ciobanu C V, Chan T L, Chuang F C, Wang C Z and Ho K M 2007 *J. Phys. Chem.* C **111** 7933–7
[22] Yang X-B, Zhao Y-J, Xu H and Yakobson B I 2011 *Phys. Rev.* B **83** 205314
[23] Lu H-D, Zhao Y-J, Yang X-B and Xu H 2012 *Phys. Rev.* B **86** 085440
[24] Landt L, Klünder K, Dahl J E, Carlson R M K, Möller T and Bostedt C 2009 *Phys. Rev. Lett.* **103** 047402
[25] Wang F and Landau D 2001 *Phys. Rev. Lett.* **86** 2050–3
[26] Zhou C, Schulthess T, Torbrügge S and Landau D 2006 *Phys. Rev. Lett.* **96** 120201
[27] Kresse G and Hafner J 1993 *Phys. Rev.* B **47** 558–61
[28] Kresse G and Hafner J 1994 *Phys. Rev.* B **49** 14251–69
[29] Kresse G and Furthmuller J 1996 *Phys. Rev.* B **54** 11169–86
[30] Kresse G and Furthmuller J 1996 *Comput. Mater. Sci.* **6** 15–50
[31] Heyd J, Scuseria G E and Ernzerhof M 2003 *J. Chem. Phys.* **118** 8207
[32] Heyd J, Scuseria G E and Ernzerhof M 2006 *J. Chem. Phys.* **124** 219906
[33] Paier J, Marsman M, Hummer K, Kresse G, Gerber I C and Angyan J G 2006 *J. Chem. Phys.* **124** 154709
[34] Paier J, Marsman M, Hummer K, Kresse G, Gerber I and Ángyán J 2006 *J. Chem. Phys.* **125** 9901
[35] Madelung O 2004 *Semiconductors: Data Handbook* (Berlin: Springer)
[36] Wu Z, Neaton J B and Grossman J C 2008 *Phys. Rev. Lett.* **100** 26804
[37] Neaton J B, Grossman J C and Wu Z G 2009 *Nano Lett.* **9** 2418